Journal of Theoretical and Applied Mechanics, Sofia, 2014, vol. 44, No. 2, pp. 25–40

SOLID MECHANICS

LENGTH-SCALE EFFECTS AND MATERIAL MODELS AT NUMERICAL SIMULATIONS OF NANOINDENTATION OF A METALLIC ALLOY*

N. Nikolov
Institute of Mechanics, Bulgarian Academy of Sciences,
Acad. G. Bonchev St., Bl. 4, Sofia 1113, Bulgaria,
e-mail: n.nikolov@imbm.bas.bg

T. Avdjieva
Faculty of Physics, University of Sofia "St. Kliment Ohridski",
5, J. Bourchier Blvd, 1164 Sofia, Bulgaria,
e-mail: tavdjieva@phys.uni-sofia.bg

I. Altaparmakov
Faculty of Applied Mathematics and Informatics, Technical University-Sofia,
8, St. Kl. Ohridski Blvd, 1756 Sofia, Bulgaria,
e-mail: ialt@tu-sofia.bg

[Received 12 February 2014. Accepted 10 March 2014]

Abstract. Some specially designed metallic alloys crystallize during process of rapid quenching which aims their amorphization. Nevertheless, change in their mechanical properties could be seen compared to these obtained during conventional technological regimes of cooling. That attracts the attention in this elaboration. Full 3-D numerical simulations of nanoindentation process of two material models are performed. The models reflect equivalent elastic and different plastic material properties. The plastic behaviour of the first one is subjected to yield criterion of Dracker-Prager and this of the second one to yield criterion of Mises.
The reported numerical results depending on the nanoindentation scale length of 1000 nanometers, suggest different adequacy of the two yield criteria to the data obtained experimentally with a Zr-Al-Cu-Ni-Mo alloy. It could be speculated that the different effects developed depending on the indenter travel of 1000 nanometers and taken into account in the two yield criteria stand behind this fact and determinate three structural levels of plastic deformation.
Key words: Nanoindentation, material models, FEM-simulations, deformation stages.

*Corresponding author e-mail: n.nikolov@imbm.bas.bg

1. Introduction

1.1. The state of art

The amorphous and the nanocrystalline-structured metallic materials are attractive in science and industry. In order to find an optimal material for a given industrial task it is essential to produce corresponding structures and to investigate, model, and analyze their mechanical properties. These materials' properties depend strongly on these structures. Investigations of the mechanical characteristics could be carried out in nano-, micro-, mezo-, macro-length scales [1]. The mechanical behaviour of solids in each of these scale-levels is determined by specific mechanisms of elastic-plastic deformation [2, 3]. They are strongly related to the definite chemical content and depend on the technological regimes of obtaining of the material's structure. Various yield criteria could be applicable in metallic materials to describe the observed effects. In the amorphous metals the classical Mises criterion has been applied [4, 5] but no so widely as the Mohr-Coulomb criterion [5, 6] and Drucker-Prager criterion [7, 8, 9]. The last two describe pressure dependent plastic flows and suggest similarity of amorphous and nanocrystalline structured metallic materials with granular materials.

At the recent time, the nanoindentation process is maybe the unique widely applied method which is able to present experimental data about the mechanical behaviour of given material at nanolevel [1, 10]. Besides the tip wearing, during a real physical experiment of nanoindentation the read data "indenter forces – indenter displacements" are influenced by different external factors, for example: the depth of initial stamp, heat difference, stiffness of the power contour, forming of pile-up and sink-in along the stamp line, scale effect of the hardness, surface roughness, recovering internal stresses, material's surface inhomogeneity, vibration influences *etc.* A numerical simulation of nanoindentation avoids a significant part of the pointed out external factors and at the same time gives an opportunity to precisely retrace the behaviour of the investigated material depending on the given material model. On the other hand, the applied material models propose opportunities to observe influence of specific effects reflected by them.

1.2. Background

A technology of design and obtaining of amorphous and nanocrystalline metallic alloys is described in [11]. It is based on the rapid quenching of melt with aims to fix its high-temperature amorphous state. To form nanocrystalline structures the obtained amorphous material is subjected to annealing. Here, it should be noted that some of the nanocrystalline phases could be ob-

tained as quenched-in phases, while the others are formed as results of the annealing process. A series of Zr-based compositions possessing aptitude to amorphization is designed and presented in [12]. Experimentally, additions of small, average and large atoms Co, Mo, Hf, respectively, in 1, 5 and 10 At% (atomic percents) are added to a Zr-Al-Cu-Ni-alloy with aims to observe the influence of the atomic radius, atomic percent of additions and the mass of alloy on the aptitude to amorphization, nano-crystallization and consequent mechanical behaviour of as the designed new materials. The obtained structures were observed as they are obtained through X-ray diffraction and SE Microscopy [13]. It is established that additions of smaller and larger atoms (Co and Hf, respectively) lead to amorphization. An increasing tendency to in-situ crystallization appears with increasing additions of the average Mo-atoms from 5 to 10 at% (atomic presents). Interacting with the larger and smaller atoms the average in size Mo-atoms could be a precondition for formation of unique atomic configurations. Hence, they could lead to specific mechanical and other properties.

1.3. Aims of the elaboration

Taking into account the above, basic aims of this elaboration are to describe and compare the material's behaviour at nanoindentation through two materials' models based on two well popular yield criteria, the Drucker-Prager's and classical Mises's. Other aims are to investigate numerically and to establish possible variation in material's response depending on variation in some parameters of the models. Additionally, based on analyzes of observed numerical effects, the elaboration aims to make some conclusions concerning operations of probable mechanisms of plastic deformation. In the sequel, the obtained two numerical indenter diagrams "Force–Travel" are compared to a real experimental one. The experimental diagram is obtained by nanoindentation of a Zr-Al-Cu-Ni-alloy containing 10% Mo-addition. This alloy is initially obtained with a crystalline structure [10] under conditions aiming amorphization by rapid quenching.

2. Theoretical bases. Nano-scale aspects at studding mechanical behaviour of plastically deformable metallic samples

It is known, that in absence of external loads the metallic atoms oscillate around an equilibrium state with amplitude 5–10% of the interatomic distance and frequency about 10^{13} s^{-1} [14, 15]. The interatomic forces are variable in accordance with the interatomic distance which is depended on the atomic radii. The initial purely elastic deformation is due to additional atomic move-

ments caused by the indenter pressure on the sample surface. These additional movements are commensurable with the distances at which the interatomic forces act. That could provoke irretrievable movements of atoms and as results irreversible deformation. The observations performed during nanoindentation reveal availability of few stages in the development of the deformation process [1, 10].

In the initial stages of nanoindentation, when the indenter displacements are in the range from few nanometers to few tens and maximum to 100 nanometers, the contact stresses play an important role. After this first stage of pure elastic deformation, the increasing contact stresses provoke initiations and movements of structural defects in materials possessing ordered crystal structures. After the advance of this second stage, the theories of loss of elastic stability of the crystal lattice and initiation, movement and erasing of structural defects in the field of elastic stresses become applicable. At nano-scale levels a special studying of this stage is imposed by the prevailing atomic mechanisms of plastic flow which are completely different from the classical. The subsequent increase of pressure force invokes a large dissemination of plastic deformation plus significant warping in the elastic stress field under the indenter. In this case, the elastic and plastic strains under the contact area should be simultaneously taken into account, because their parts in the total deformation become now comparable. That could be successfully performed by a numerical simulation of the nanoindentation process through the Finite Element Method, for example.

3. Models of materials

A conclusion could be derived from the previous section that since different deformation stages have been observed it should be followed that at different deformation levels, different deformation mechanisms operate determining the levels. These mechanisms having elastic, plastic or mixed characters should assure corresponding material's response to the external loads so that both the continuity of plastic flow and the non-compromising of the sample to be kept.

In this Section, the mechanical behaviour at nanoindentation of the two material models based on the two criteria will be numerically modelled. The behaviour of metallic alloy is modelled as elastic-plastic independent on the strain rate applying FEM and commercial program product Ansys. The elastic behaviour is characterized by strains proportional to increasing stresses. The plastic behaviour is characterized by sharp appearance of irreversible deformation with smooth achievement of stresses until yield stress value σ_y. The values

σ_y is not depended on the time and is a characteristic of the given material. This value is determined by yield criteria. The three elements building such a material model include: yield criterion $F(\boldsymbol{\sigma}, \kappa, \boldsymbol{\alpha}) = 0$, where $\boldsymbol{\sigma}$ is stress vector, κ is plastic work consumed during the whole process of loading and $\boldsymbol{\alpha}$ is movement of the yield surface depending on the history of loading, the flow rule and the hardening rule. In the here-build two numerical models of nanoid-netation material behaviour, the applied yield criterion of Drucker-Prager (3.1) and yield criterion of Mises (3.2) are reduced to nano-scale level and have the well-known classical expressions [4 - 9] in principal stresses $\sigma_1 \geq \sigma_2 \geq \sigma_3$:

$$(3.1)\quad F \equiv \frac{1}{6}\sqrt{(\sigma_1-\sigma_2)^2+(\sigma_2-\sigma_3)^2+(\sigma_3-\sigma_1)^2} - \alpha_1(\sigma_1+\sigma_2+\sigma_3) = k_1,$$

$$(3.2)\quad F \equiv (\sigma_1-\sigma_2)^2+(\sigma_2-\sigma_3)^2+(\sigma_3-\sigma_1)^2 = 6k^2 = 2\sigma_y^2.$$

In (3.1), the cohesion of the material $k_1 = \dfrac{\sigma_y\sqrt{3}(3-\sin\varphi)}{6\cos\varphi}$ and the material constant $\alpha_1 = \dfrac{2\sin\varphi}{\sqrt{3}(3-\sin\varphi)}$ dependant on the angle of internal friction φ are determined experimentally. In (3.1) and (3.2), σ_y is the yield stress but defined depending on the cohesion and internal friction (3.1) and defined under uniaxial tension (3.2), and in (3.2) $k = \sigma_y/\sqrt{3}$. The material model based on Drucker–Prager yield criterion does not possess hardening rule. The hardening rule in the material model based on Mises yield criterion is described by Model of Bilinear Isotropic Hardening.

In the **Model of Bilinear Isotropic Hardening**, the yield criterion of Mises is applied with associative plastic flow rule and isotropic work hardening. The material model is set by Elastic modulus E, Poisson's ratio ν, yield stress σ_y, tangential modulus T. During the indentation process the actual yield stresses are directly determined through the equivalent plastic strain in the "stress-strain" diagram at one-axial tension since at work hardening the yield stress is a function of the work consumed for plastic deformation.

In the **Model of Drucker –Prager without hardening** the yield criterion of Drucker-Prager is applied with associative plastic flow rule. The yield surface is not variable with the development of plastic flow. Hence, it follows that there is no hardening rule and the material is elastic-perfectly plastic. The material's model is set by coefficient of cohesion k_1, angle of internal friction φ and dilatancy angle φ_f. Coefficient k_1 and angle φ are determined experimentally, and so that the yield surface must present a circle cone around the

six-wall cone determined by the yield criterion of Mohr-Coulomb. The yield stress limit is defined through the definition of constant k_1 as:

$$\sigma_y = \frac{6k_1 \cos\varphi}{\sqrt{3}(3 - \sin\varphi)}. \tag{3.3}$$

In this case, the equivalent stress is interpreted as equivalent stress of Mises at plastic flow with yield stress limit of the actual hydrostatic stress.

In the two models, the indenter's material is modelled as diamond possessing Young's modulus $E = 1141$ GPa and Poisson's ratio $\nu = 0.07$.

An elastic-perfectly-plastic material with $E = 88.8$ GPa and $\nu = 0.36$ is assumed for the sample modelled according to Drucker-Prager model. The plastic behaviour is modelled by the three parameters cohesion, friction angle, dilatancy angle. In this elaboration, the influence of the three constants on the character of the obtained diagrams "force-travel" and on the plastic behaviour, respectively, is investigated through the assignation of 548.5 MPa for the cohesion and equal values for the angles from -2, 0, 2, 5 to 10°.

The elastic-plastic hardening behaviour of the second material based on Mises criterion is described by the same elastic characteristics $E = 88.8$ GPa and $\nu = 0.36$. The plastic behaviour is described by yield stress limit σ_y and tangential modulus T. The influence of both the characteristics on the nanoindentation material's behaviour is investigated by assignation of variable yield stress $\sigma_y = 633.53$ and 1720 MPa and for T from 70 to 130 MPa and 300 MPa. The value 633.53 MPa corresponds to $k_1 = 548.5$ with $\varphi = 0^\circ$ according to (3.3).

4. Modelling of material behaviour at nanoindentation process

Two full 3-D model of the nanoindenter compression process in an experimental sample is developed applying the presented material models and taking into account the nano-scale aspects at metal plastic deformation. In the first model, the sample possesses elastic-plastic behaviour described by the yield criterion of Drucker-Prager, and in the second by criterion of Mises.

The indenter has a three angular equal-walls pyramidal form of Bercovich with a pin angle 70.3° and radius 70 nanometers. In the two models, the indenter is meshed in 607 and 601 SOLID95 finite elements with 1316 and 1308 nodes, respectively. The element mesh is refined at the indenter pin. The sample has form of parallelepiped with high 5000, width 5000 and length 10000 nanometers. At the modelling following Drucker-Prager criterion, the sample

contains 38020 finite elements SOLID95 and following Mises 59607 finite elements VISCO107 and contains 54434 and 11242 nodes, respectively. The mesh is also refined in the contact area. Finite elements VISCO107 are defined by 8 nodes, placed in the 8 vertexes of a parallelepiped form and possess three degrees of freedom – displacements along the axes for each node. Finite element SOLID95 is defined by 20 nodes. Each node has three degrees of freedom along the axes, also. The SOLID95 has parallelepiped form with nodes in edge centers besides the elements in the vertexes. The elements can describe plasticity, creep, stress stiffening, large deflection, and large strain capabilities.

Standard contact conditions of Coulomn friction model with 235 contact elements TARGE170 on the indenter for the two models and 2098 and 3142 contact elements CONTA174 on the sample are set, respectively. The contact surfaces are in sticking and support equivalent tangential stresses up to the values $\tau = \mu p + C$, where $\mu = 0.1$ is friction coefficient, p is contact pressure and $C = 0$ is cohesion sliding resistance, here assumed with default value 0, before a relative sliding between the indenter walls and the sample surface to begin. The sticking-sliding calculations determine when a point transits from sticking to sliding. In this way, an opportunity appears not only to describe a form of the contact stamp surface, but also to fit numerically this surface according to an experimentally obtained form. After, the relation "force-travel" for the indenter could be searched according to reverse methods.

The loading process is simulated by step displacement of the indenter from 0 to 850 nanometers. After, reverse displacement of the indenter is given simulating unloading process. The computations are performed in 24 steps. During the loading up to the first 50 nm, the indenter travel increases with 10 nanometers per step and after the travel 50 nm with 50 nm per step up to coming at 850 nm. The sample is unloaded in three steps with travel of 50 nm per each step. The dependency "force-travel" is read.

5. Numerical results

The diagrams "force-travel" obtained with cohesion 548.5MPa and equal values $-2°$, $0°$, $2°$ for the two angles are given in Fig. 1 for indenter travel up to 600 nm. The read values for the force are 22.174, 24.120 and 26.075 mN, respectively. It is seen, the indentation force increases with increasing angles. With the same cohesion for the same travel and angles $5°$ and $10°$ the force is 29.511 and 36.404 mN. The increasing cohesion also leads to increasing indentation force. With travel 850 nm the maximal force is 38.251 mN. Irreversible deformation appears after unloading from 600 and 850 nm. The yield stress

could be $\sigma_y^{D-P} = 633.35$ MPa with $\varphi = \varphi_f = 0°$ and cohesion $k_1 = 548.5$, according to the model based on Drucker-Prager's yield criterion. But here, the equivalent stresses are now computed in relations with the material's cohesion (3.1) i.e. cohesion of molecules, atoms, ions in a physical body under the action of attractive forces, because the yield stress results from this cohesion, but not from the yield stress resulting from the one-axial tension diagram (3.2) as it was in the Bilinear model of isotropic hardening with Mises's yield criterion.

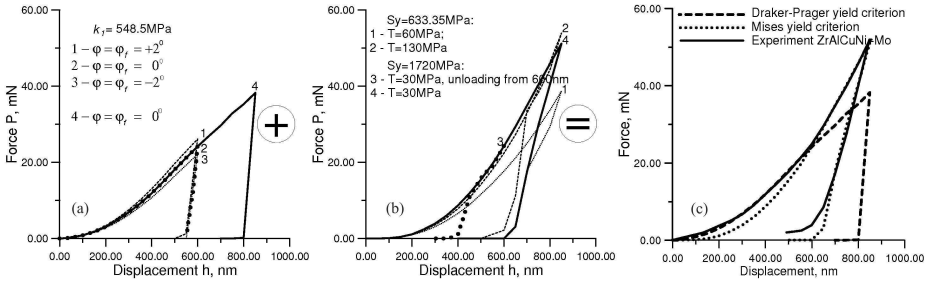


Fig. 1 Material's response at nanoindentation, numerically modelled (a) by Drucker-Prager yield criterion; (b) by Mises yield criterion and (c) compared, dashed lines, with a real response identified experimentally, solid line

The applied loading conditions are analogical to these at the model based on Drucker-Prager criterion without hardening during the numerical simulation of nanoindentation of a material possessing plastic behaviour based on yield criterion of Mises with associative flow rule and isotropic work hardening. During the loading, the computations are accomplished in 21 steps and during the unloading in 7 steps. Between 850 and 700 nm the step-travel size is 50nm, and it is 100 nm during unloading from 700 to 400 nm.

In Fig. 1(b) the obtained "force-travel" diagrams are presented. As it was in the previous case, the sample is firstly loaded up to indenter travel 600 nm and after it is unloaded. Completely different mechanical behaviour is observed in comparison to the first model. By the choice of 633.53 MPa for yield stress, under equal other conditions a logical transition is performed from the first model to the second in order to retrace the behaviour of the two models depending on the yield criteria under equal plastic properties. In comparison to the first model, a smaller plastic deformation is read together with the enforced elastic. That is caused by the values of the tangential modulus T. The relation between both the modules elastic and tangential could be defined by the known dependencies of Ramberg-Osgood. At elastic deformation, the tangential modulus is equal to the elastic one (Young's). The slope varied

with initiation of plastic deformation and could be a characteristic of the ratio elastic/plastic deformation in the total deformation. Generally, the tangential modulus characterizes the material's hardening after the beginning of plastic transition in plastic state. The work hardening (named also strain hardening or cold working) in crystal structure increases the mechanical characteristics owing to the dislocation generation and movement, their bifurcation, branching, coalescence, stopping or coming to surface, or erasing. That is a measure for ability of material structures to remain in plastic state and to keep the material's continuality. An increase of compression force is read with increasing T to 70, 90, 110, 130 and 150 MPa. With increasing T over 100MPa, a pure elastic deformation is observed after unloading from indenter travel 850 to 700 nm, Fig. 1(b), curve 2. This pure elastic deformation disappears with increasing yield stress. With $\sigma_y = 1720$ MPa, decrease of T to 30 MPa and travel 850 nm the maximal force is 51.16614 mN. The deformation possesses elastic-plastic character after unloading. The depth of contact stamp is 640-650 nm. With the same characteristics and travel 600 nm after unloading the maximal force is 24.205 mn. The depth of contact stamp is 350 nm. The "unloading" curve has a clearly expressed elastic part at travel from 600 to 400 nm. This part is followed by second elastic-plastic part. A comparison of curve 3, Fig. 1(b), to curve 2, Fig. 1(a), reveals that two approximately equal compression forces of 24.12074 and 24.205 mN obtained with equal indenter travel of 600 nm produce different effects in the two models, shown in Figs 2 and 3. The registration of such effects could indicate transition of the material's response from nano- to micro-hardness. Mezzo- and macro-hardness could be registered over travel 850–1000 nm.

6. An interpretation of the numerical results. Discussion

In Fig. 1(c), a generalization of curves 4 belonging to Figs 1(a) and 1(b), dashed lines, and a comparison to an experimental result of nanoindentation of Zr-Al-Cu-Ni-Mo-alloy, solid line, are presented.

It is read that with the simulation of indenter travel up to 600 nm, the obtained numerical "force-travel" dependency according to Dracker-Prager criterion coincides with the experimental one. After work travel 600 nm, the simulated deformation behaviour is different from the experimental one. At the material model based on the Mises criterion, the difference in material behaviour is observed with the indenter travel smaller than 600 nm. After this travel, accordance with the experimental curve is seen. The variation of the materials parameter in both the models, Figs 1(a) and 1(b), leads to deviation

of the numerical curves from the experimental one. The diagram could be divided in three intervals at loading. Compared to the experiment they could be supposed as identical with stages in the development of deformation process. These are the intervals from 0 to 200–250–300 nm, from 200 to 600 nm and from 600 to 850 nm.

It is seen, Fig. 1(a), that during the second stage the numerically modelled behaviour based on Drucker-Prager criterion is adequate to the experimentally observed. It is also seen, Fig. 1(b), that during the third stage with the plastic strain development the numerically modelled behaviour based on Mises's criterion is adequate to a real process of loading. The behaviour during unloading, Fig. 1(b), is also adequate to a real behaviour at unloading of the same real metallic sample.

Since at the first model the used Dracker-Prager yield criterion describe strains developed as a result of influence of the principal stresses, a conclusion could be made that the observed result up to travel 600 nm is related to them. The material is characterized by elastic-perfectly-plastic behaviour. Such a behaviour is described by material cohesion and both angles of friction and of dilatancy. With both the angles equal or close to 0 the conclusion might be drawn that as simulated mechanical behaviour of this metallic material is analogical to behaviour of a material composed of granules possessing cohesion of 548.5 MPa.

Looking at the Fig. 1 and taking into account the fact of coincidence, the conclusion could be made that beginning with indenter travel from 200–250 nm, the plastic deformation mechanisms are analogical to these ones acting in granularly-structured materials. Since the used in this case Drucker-Prager yield option is applicable to granular (or frictional) materials, it could be logically to explain the observed behaviour as a caused by deformation mechanisms similar to these acting in these materials, but requiring significantly more deformation energy. Such materials are characterized with loss of energy during the interaction between their constituents. The structures of such a material should be sufficiently large in sizes, so that they do not permit to be subjected to thermal motion fluctuations. Else, phase transformations in the material could begin as a result of friction and increasing temperature. Thus, the lower size limit for grains in a granular material is about 1 micrometer. In that sort of case, the crucial is the bonding forces among the different materials' constituents (or aggregates), which could be identified at the corresponding size level, as well as, their form, boundary layers and friction conditions between them. In the first model, the presence of plastic deformation without hardening could be explained by change in the forms or/and the situations of the materi-

als particles. Some transpositions in materials structures might be registered. A developed classical plastic deformation, as it is well-known in the metals, induced by classical mechanisms acting in micro-, meso- and macro-levels should not be registered.

After the travel of 600 nm, the material's behaviour is determined by the difference in the principal stresses only. Other plastic deformation mechanisms are triggered in the place of the cohesive ones. The operating mechanisms are suspended and give the places of others. The cohesion influence decreases with increasing indenter travel. Influence of work hardening described by the tangential modulus T advances. During unloading from 850 nm, the simulation based on Mises's criterion shows an elastic-plastic recovering and coincides with the experiment.

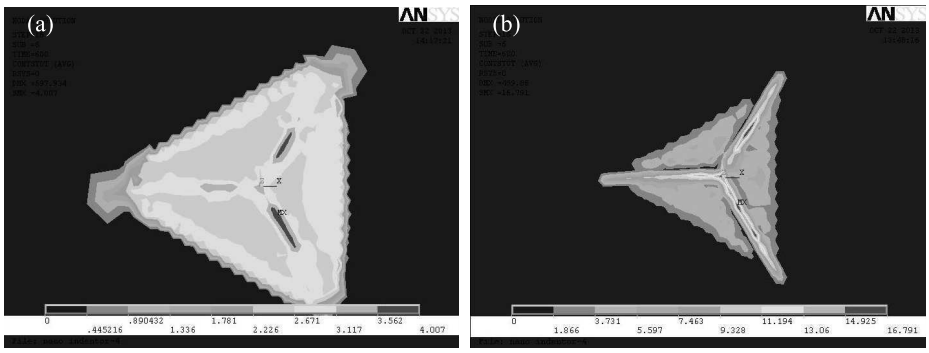


Fig. 2. Contact stress distribution obtained with indenter travel 600 nm (a) in the model based on Drucker-Prager's yield criterion without hardening and (b) in the model based on Mises's yield criterion with linear hardening

The analysis of the behaviour of the two materials with indenter travel 250–600 nm reveals that the two compression forces 24.120 and 24.205 mN, obtained with one and the same travel, lead to different material's response. That is reflected by the distributions of contact stresses, equivalent stresses and the total strain. In Fig. 2, the contact stress distributions are presented. With the applied Coloumn's contact friction model, concentrations of the maximums around the indenter edges are observed for both materials. At first, the maximal are in the range of 3.56–4 MPa, Fig. 2(a), and at the second 14.92–16.79 MPa, Fig. 2b. The contact areas possess a triangular form. The surface triangle has larger area at the first model, and for the second it has concave sides. For both cases, the prevailing contact stresses have one and the same order on the ranges of 2.226–2.671–3.117 MPa and 3.731–5.597 MPa. At the second

model, a decrease to 1.066 MPa exists before the edges and behind them stress concentrations are seen on the ranges of 7.463–9.328–11.194 MPa, Fig. 2(b). At the first model, with increasing distance from the indenter pin to the periphery, the contact stresses firstly decrease from 2.671 to 2.226 MPa, and after they increase in opposite order. Similar distributions established numerically could be seen in [4], and similar stamp forms are experimentally observed in [9, 10].

The distributions of the equivalent stresses obtained by Drucker-Prager criterion given in Fig. 3(a) display a plastic flow with stresses 1017–1162 MPa developed in a round area to the indenter. In this area, an other triangular area with lower stresses, close to the yield stress limit calculated with zero-angles of friction and dilatancy on the ranges of 582–727 MPa concentrated in round parts, is observed. Such wavy areas typical of granularly-structured materials are observed experimentally and numerically in [4]. From this fact, a conclusion could be derived that with indenter travel up to 600 nm the material based on Drucker-Prager yield criterion demonstrates behaviour similar to this of a granularly-structured material with values of cohesion 548.5 MPa but without internal friction. A relation with Fig. 4, where the stamp profile in depth obtained with the same travel is presented, displays the presence of higher wavy parts, the so called pill-ups, in this area.

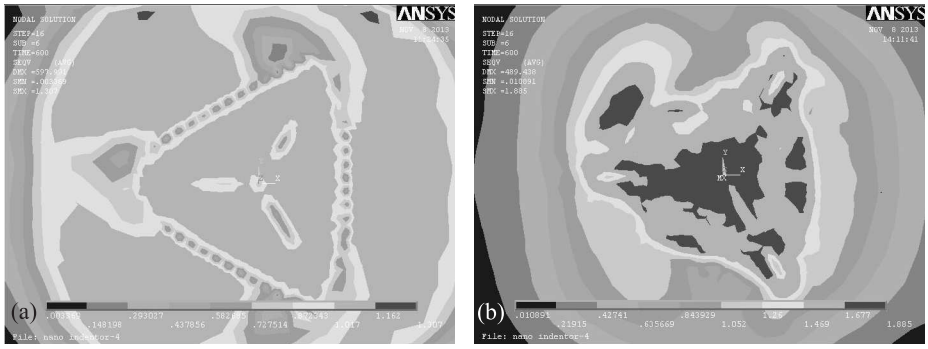


Fig. 3 Equivalent stress obtained with indenter travel 600 nm (a) at modelling with Drucker-Prager yield criterion without hardening and (b) at modelling with Mises yield criterion with linear hardening

At the model based on Mises's criterion, similar rough the so called sink-ins are observed on the stamp walls. The distribution of the equivalent stresses given in Fig. 3(b) shows a triangular type on the ranges of 1469–1677–1885 MPa. Here, in the second subinterval, the values close to the yield stress limit are observed, which suggests that after 600 nm developed plastic flow

exists it this model. It is determined by the differences in the principal stresses following the Mises's criterion. That is illustrated by the stress concentrations in single areas, as well as the values of maximal stresses with travels 550 and 650 nm, respectively. The plastic strain initiation at the material based on Mises criterion begins with travel 250–300 nm. Up to this travel, the material appears in elastic state according to the assumed model.

In Fig. 4, the numerically obtained stamp profiles after unloading from 600 and 850 nm are presented. The right part of the curves corresponds to the middle part of the wall and the left part corresponds to the opposite edge following the section along the horizontal plane XZ, Figs 2 and 3. It is seen, that at an elastic-perfectly-plastic material modelled by SOLID95 finite elements and Drucker-Prager flow rule, the stamp form copies the indenter form. The residual depth approximates to the assigned indenter travel since there is no hardening of the material after unloading. That could be explained by translations and/or rotation of structured elements situated close to the surface of real sample.

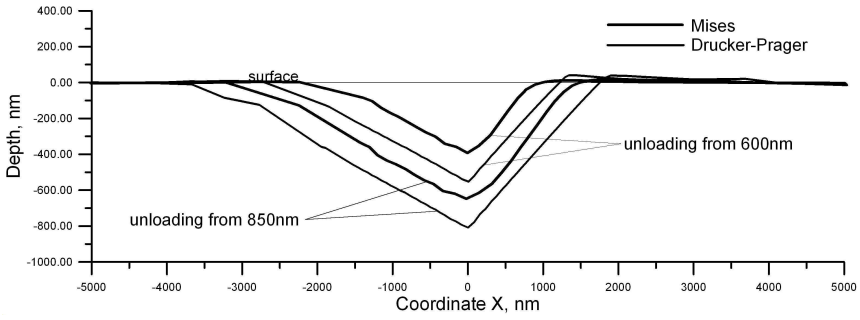


Fig. 4. Profiles of the numerically obtained indenter stamps after unloading from 600 and 850 nanometers

These "materials' responses" are caused by the compression on the indenter and the friction on its walls described by the contact friction model of Coulomn. Influence of the elastic strain is observed at the elastic-plastic material with isotropic work hardening and modelled VISCO107 finite elements. The profile depth is 400 and 650 nm, approximately for the two travels. The wavy deviations from plainness of the stamp surfaces contacting with the indenter could be related to irreversible deformation after unloading. Waves are not observed on the free non-contacting surface of the sample i.e. it does not undergo plastic deformation by reason of a granular structure and cohesion as it is with the first model.

A comparison with the experimental diagram, Fig. 1c, shows that under unloading of the second model the numerically modelled behaviour coincides with the experimentally observed one. The presence of elastic recovering, Fig. 4, presumes larger influence of elastic deformation mechanisms during unloading than in the previous case.

7. Conclusions

Two materials' models of mechanical behaviour at nanoindentation are developed by an application of Drucker-Prager yield criterion with associative plastic flow rule without hardening and by an application of Mises yield criterion with associative plastic flow rule and isotropic work hardening. The numerical investigations accomplished by variation of the plastic parameters under equivalent elastic characteristics (Young's modulus 88.8G Pa and Poisson's ratio 0.36) display increasing compression indenter forces for the two models: at the first model with increase of the cohesion over 548.5 MPa and both the equal angles of fiction and dilatancy from -2°, 0°, 2°, 5° to 10°, and at the second model with increasing yield stress limit from 633.35 to 1720 MPa and increasing tangential modulus from 30, 60 to 130 MPa.

Elastic-perfectly-plastic behaviour is established depending on the cohesion and the two angles of fiction and dilatancy during the loading of the model based on Drucker-Prager criterion up to 600 nm. During unloading of this model, one and the same constant low elasticity, independed of both the angles, is established. An identical elastic-plastic behaviour is established under loading and unloading of this model up to 850 nm.

Variable elastic behaviour with two different elastic modules is established at the second model based on the Mises yield criterion with high yield stress limit of 1720 MPa and low tangential modulus of 30 MPa, under unloading from 600 nm. At the unloading from 850 nm, the model shows elastic recovering, characterized by one constant modulus. This recovering could be described by one elastic characteristic. The increase of the tangential modulus to 130 MPa under lower yield stress limit of 633 MPa also leads to two-modules elastic recovering.

Three deformation stages are revealed in the real material investigated experimentally comparing the obtained numerical results "Indenter force – indenter travel" to experimental ones for a Zr-Al-Cu-Ni alloy with Mo-addition of 10at% (atomic percents) during loading. One stage is established during unloading. Based on the different plastic effects reflected by the two models, it is suggested that during the four stages different structural mechanisms of plastic deformation operate in the material volume, and that the four stages might be

assumed as equivalent ones of different structural levels of plastic deformation depending on the scale levels of investigation.

The first stage is elastic and begins with the onset of the indentation process from 0 and goes on until travel of 200–250 nm. During the second stage performed by travel from 250 to 600 nm, based on the coincidence of the numerical curve obtained according Drucker-Prager criterion with the experimental, it is assumed that transpositions in the material structure are realized but only depending on the cohesion properties of the material. During the third plastic stage, the deformation is initiated through mechanisms analogical to these operating in materials described by classical Mises criterion. The scale size increases with going on to micro-, meso, and macro- scale levels. With such an increase over 1000 nm, the influence of cohesion, as well as, the part of travel 600 nm decreases in the total work travel, so that the corresponding effects are not detectable. After, the plastic behaviour becomes describable following the Mises criterion and the mechanisms which determine corresponding tangential modules remain to operate predominantly.

For both models, the observed numerically effects could be experimentally related to the plastic deformation mechanisms operating in the different scale levels. Estimations of the effects of such mechanisms could be drawn on the basis of the constants of the here presented models.

REFERENCES

[1] Golovin, J. I. Nanoindentation and Abilities, Moscow, Mashinostroenie, 2009 (in Russian).

[2] Zhang, Z. F., J. Eckert, L. Schultz. Difference in Compressive and Tensile Fracture Mechanics of $Zr_{59}Cu_{20}Al_{10}Ni_8Ti_3$ Bulk Metallic Glass. *Acta Mater.*, **51** (2003), 1167–1179.

[3] Bahr, D. F., D. E. Kramer, W. W. Gerberich. Non-linear Deformation Mechanisms during Nanoindentation. *Acta Mater.*, **46** (1998), 3605–3617.

[4] Vaidyanathan, R., M. Dao, G. Ravichandran, S. Suresh. Study of Mechanical Deformation in Bulk Metallic Glass through Instrumented Indentation. *Acta Mater.*, **49** (2001), 3781–3789.

[5] Yu, G. S., J. G. Lin, M. Mo, X. F. Wang, F. H. Wang, C. E. Wen. Effect of Relaxation on the Pressure Sensitivity Index in a Zr-based Metallic Glass. *Mater. Sci. and Engineering A*, **460**–**461** (2007), 58–62.

[6] Baricco, M., T. A. Baser, J. Das, J. Eckert. Correlation between Poisson Ratio and Mohr–Coulomb Coefficient in Metallic Glasses. *J. of Alloys and Compounds*, **483** (2009), 125–131.

[7] Hua, J., Y. Xie. A Note on the Mohr–Coulomb and Drucker–Prager Strength Criteria. *Mech. Res. Commun.*, **38** (2011), 309–314.

[8] Feng, L., Y. Kang, G. Zhang, S. Wang. Mechanism-based Srain Gradient Drucker–Prager Elastoplasticity for Pressure-sensitive Materials. *Int. J. of Solids and Structures*, **47** (2010), 2693–2705.

[9] Fornell, J., A. Concustell, S. Suriñach, W. H. Li, N. Cuadrado, A. Gebert, M. D. Baró, J. Sort. Yielding and Intrinsic Plasticity of Ti–Zr–Ni–Cu–Be Bulk Metallic Glass. *Int. J. of Plasticity*, **25** (2009), 1540–1559.

[10] Oliver, W. C., G. M. Pharr. An Improved Technique for Determining Hardness and Elastic Modulus using Load and Displacement Sensing Indentation Experiments. *J. Mater. Res.*, **7** (1992), No. 6, 1564–1583.

[11] Nikolov, N. Technology of Nanocrystalline-structured Materials obtained through Glass-transition of Amorphous Metallic Alloys. In: Series in Applied Mathematics and Mechanics, No. 3, Institute of Mechanics–BAS, Sofia, 2012, 3–35.

[12] Nikolov, N. Mathematical Models of Tg and Tx, and Search for Maximal Supercooled Liquid Regions ΔTx for Zr-Al-Cu-Ni Glassy Alloys. *Technical Ideas,* **XLI** (2004), 67–79.

[13] Avdjieva, T., N. Nikolov. X-ray Diffraction and SEM Observations of Zr-Al-Cu-Ni Amorphous Alloys Containing Mo-additions. *Compt. Rend. de l'Acad. Bulg. des Sci.*, **64** (2011), 1743–1748.

[14] Li, J. H., Y. Dai, X. D. Dai. Long-range N-body Potential and Applied to Atomic Modelling the Formation of Ternary Metallic Glasses. *Intermetallics,* **31** (2012), 292–320.

[15] Eberhart, M. E. The Metallic Bond: Elastic Properties. *Acta Mater.*, **44** (1996), 2495–2504.